Correcting magnetic probe perturbations on current density measurements of current carrying plasmas

P. Knoblauch,[1,a)] V. Raspa,[1] F. Di Lorenzo,[1] A. Lazarte,[1] A. Clausse,[2] and C. Moreno[1]
[1]*Departamento de Física, FCEyN-UBA, PLADEMA-CNEA, and INFIP-CONICET, Pab. 1, Ciudad Universitaria, 1428 Buenos Aires, Argentina*
[2]*PLADEMA-CNEA, and CONICET, Universidad Nacional del Centro, Campus Universitario, Paraje Arroyo Seco, 7000 Tandil, Buenos Aires, Argentina*

(Received 14 May 2010; accepted 28 July 2010; published online 20 September 2010)

A method to infer the current density distribution in the current sheath of a plasma focus discharge from a magnetic probe is formulated and then applied to experimental data obtained in a 1.1 kJ device. Distortions on the magnetic probe signal caused by current redistribution and by a time-dependent total discharge current are considered simultaneously, leading to an integral equation for the current density. Two distinct, easy to implement, numerical procedures are given to solve such equation. Experimental results show the coexistence of at least two maxima in the current density structure of a nitrogen sheath. © *2010 American Institute of Physics.*
[doi:10.1063/1.3480556]

I. INTRODUCTION

Plasma focus devices offer excellent opportunities for conducting research on dense plasmas and their applications. Essentially, such devices operate by generating an intense electrical discharge between two cylindrical coaxial electrodes located in a low pressure chamber. Under suitable conditions, a hypersonic current sheath is produced that is accelerated by the Lorentz force toward the open end of the electrodes. The sheath ultimately collapses radially on the electrodes axis of symmetry generating a dense plasma focus from which different radiations are profusely emitted. Many important applications such as microlithography and micromachining,[1–4] surface technology,[5–8] and flash radiography,[9–15] among others, were proposed and developed for those radiations. When used with deuterium or deuterium-tritium mixtures, fusion neutrons are also emitted, widening the field of potential applications.[11,15,16]

Since the device performance is strongly influenced by the formation and evolution of the current sheath, it is of interest to investigate its structure and dynamics. Several experimental methods were developed to measure the plasma sheath properties during the different stages of the discharge. Optical techniques such as shadowgraph and Schlieren photography, interferometry, and Faraday rotation, for instance, are attractive since they are nonperturbative, but their drawback is that they integrate the plasma behavior along the sight line, and therefore numerical methods are needed to infer local information from the measured data.

Magnetic probes, in turn, although being intrusive, provide local information about the magnetic field associated with the current sheath and can give useful information on the current density structure, provided that the appropriate corrections are made. Current redistribution due to the presence of the probe and the fact that the probe itself can eventually sense the temporal variation of the magnetic field related to the time varying discharge current are among those perturbations that need to be corrected.

The distortions on the probe signal caused by current redistribution were examined in Refs. 17 and 18 under the assumption of a time independent discharge current, and the effect of a time dependent discharge current was investigated in Ref. 19 assuming a negligible current redistribution.

In the current article, a method that considers both effects simultaneously and that allows to infer the current density structure of a plasma sheath during the run down phase of a plasma focus discharge is presented. It is afterward applied to a 1.1 kJ plasma focus, taking the output signals of a magnetic probe and a nonintegrating Rogowski coil as input data.

II. INFERRING THE CURRENT DENSITY FROM THE PROBE SIGNAL

The current density profile can be inferred from the magnetic probe signal according to a model of a planar current sheath of thickness D moving at constant axial velocity u along the z-axis. The probe is at rest in the laboratory frame of reference (see Fig. 1). Further hypotheses are that all the discharge current circulates through the sheath and that there are no external sources of magnetic field affecting the sensing coil.

Considering that the coil radius is much smaller than the characteristic scale of the spatial variation of the magnetic field, the voltage $v(t)$ induced on the probe can be expressed as

$$v(t) = -A\frac{dB(t)}{dt}, \tag{1}$$

where A is the coil effective area concatenating the magnetic flux and $B(t)$ is the magnetic field component parallel to the

a)Electronic mail: pablotk@df.uba.ar.

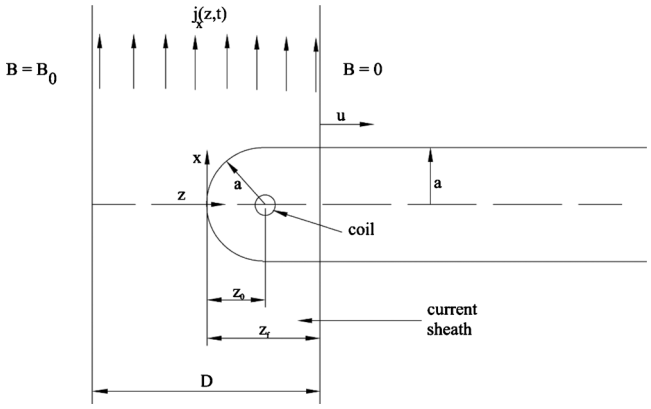

FIG. 1. Sketch of a magnetic probe of radius a with a hemispherical tip. The sensing coil is located at a distance z_o from the probe's tip. The probe is considered to be at rest in the laboratory frame of reference and that a current sheath of thickness D moving with velocity u impinges on it.

magnetic normal of the coil. Let us write the unperturbed current density $\mathbf{j}$ as

$$\mathbf{j}(z,t) = a(t) j_x(z) \hat{x}, \tag{2}$$

which represents a frozen profile $j_x(z)$ modulated by a time dependent amplitude $a(t)$. While the density profile is unknown, the current amplitude can be directly evaluated from the signal of a Rogowski coil placed so as to sense the total discharge current or its time derivative.

In order to account for the signal distortion caused by the probe's body, Bruzzone *et al.*[17] showed that, considering Eq. (2), the magnetic field at the coil position is given by

$$B(t) = \mu_o a(t) \int_0^{z_f} j_x(z - z_f, t) M\left[\frac{z_o - z}{r(z)}\right] dz, \tag{3}$$

where z_f and z_o are the distances from the probe tip to the sheath front and to the probe coil, respectively (see Fig. 1). The expression $r(z)$ describes the radius of the hole produced on the sheath by the probe as a function of the z-coordinate and $M(\xi)$ is the function

$$M(\xi) = \frac{1}{\pi}\left[\cot^{-1}(\xi) - \frac{\xi}{1+\xi^2}\right] \quad -\infty \le \xi \le \infty \tag{4}$$

derived by Malmberg[20] to express the magnetic field induced by a planar current sheath of infinitesimal width, on the axis of a circular hole produced on the sheath by the probe's body. The ξ-coordinate is measured along the axis in terms of the hole radius. Hence, in the case depicted in Fig. 1, $\xi = (z_o - z)/r(z)$. For a hemispherical probe tip of radius R, the function $r(z)$ is given by

$$r(z) = \begin{cases} 0 & \text{if } z \le 0 \\ \sqrt{2Rz - z^2} & \text{if } 0 < z < R \\ R & \text{if } z \ge R. \end{cases} \tag{5}$$

Differentiating Eq. (3) and combining with Eq. (1), the current distribution $j_x(z - z_f, t)$ results to be related with the probe signal $\nu(t)$ as

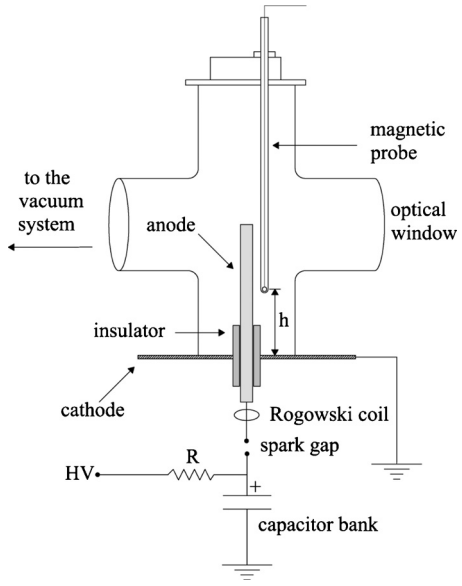

FIG. 2. Sketch of the experimental setup.

$$\frac{\tilde{\nu}(t)}{a(t)} - \frac{\dot{a}(t)}{a^2(t)} \int_0^t \tilde{\nu}(\tau) d\tau = \int_0^{z_f} j_x(z - z_f, t) \tilde{M} dz, \tag{6}$$

where $\dot{a}(t) = da(t)/dt$ and the following two quantities were introduced for the sake of notation simplicity

$$\tilde{\nu}(t) = \frac{\nu(t)}{\mu_o A u} \quad \tilde{M} = \frac{d}{dz} M\left[\frac{z_o - z}{r(z)}\right]. \tag{7}$$

The left hand side of Eq. (6) distinguishes two contributions: the first term is independent of the time variation of the discharge current amplitude, whereas the second one takes account for such temporal variation.

Equation (6) is valid as long as the current amplitude $a(t)$ is not null, that is, after the dielectrical breakdown of the filling gas and before the first half of period of the discharge current. These conditions are clearly met for cases of practical interest during the rundown phase.

Expression (6) is an integral equation for the current density profile j_x, which is a Volterra equation of the first kind that can be solved numerically.[21,22] Two numerical schemes for inferring discrete values of j_x from measured values of $\nu(t)$ and $a(t)$ are given in the Appendix.

III. DEVICE, SENSORS, AND MEASURED SIGNALS

The plasma focus capacitor bank is formed by eight units (0.7 μF each) connected in parallel surrounding both the spark gap and the discharge chamber, totalizing a connection inductance of 167 nH. The bank is charged up to 20 kV (1.1 kJ of stored energy) and delivers a peak current of 200 kA in a quarter period of 1.6 μs. The discharge chamber is a 5 l cylindrical cross, made of Pyrex glass of 10 mm thick wall. The anode is a cylindrical solid titanium bar, 9.4 ± 0.1 mm diameter, and 100.0 ± 0.1 mm length. The cathode is an aluminum disk drilled at its center, coaxially

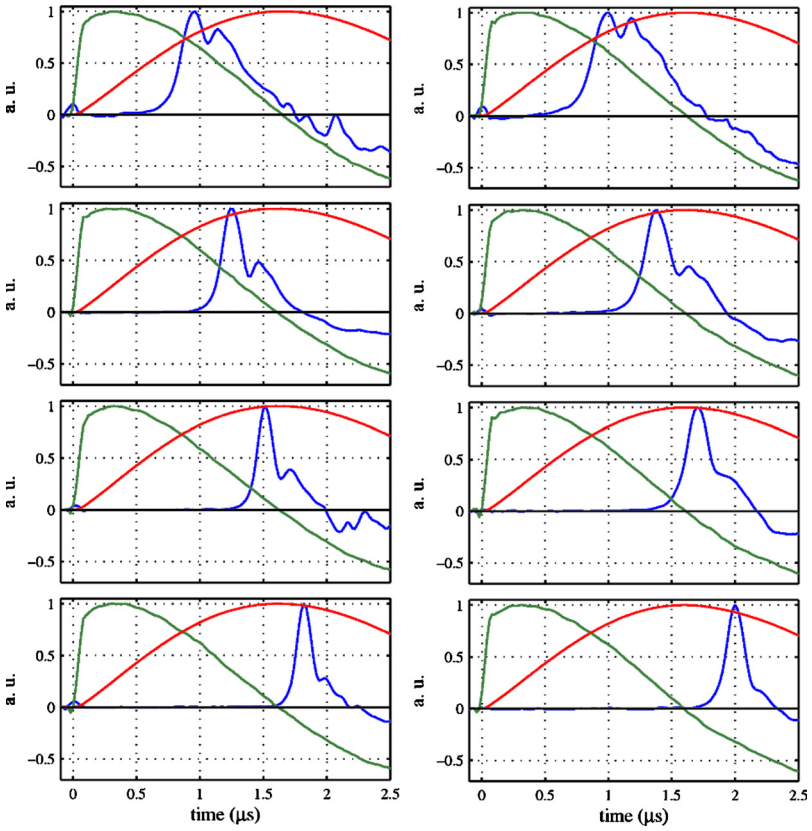

FIG. 3. (Color online) Measured magnetic probe and Rogowski signals (blue and green, respectively) for N_2 at 0.5 (left) and 1 mbar (right). The calculated total current for each case is also shown (red).

placed with respect to the anode (see Fig. 2). Both electrodes are isolated by a 1.3 ± 0.1 mm thick Pyrex tube, 10 mm high, and 12.8 ± 0.1 mm outer diameter (OD). A nonintegrating Rogowski coil and an inductive magnetic probe were used as measuring devices.

The magnetic probe case is a Pyrex glass tube, 6.0 ± 0.2 mm OD, with hemispherical tip. A 12-turns sensing coil, 1.00 ± 0.05 mm radius, is placed inside the tube close to the tip. The probe was positioned and oriented such that the sensing coil concatenates the azimuthal component of the magnetic field generated by the discharge current nearby the anode. The coil center was located at a radius of 15.5 ± 0.5 mm measured from the symmetry axis. Experiments were conducted placing the coil at axial positions of 2, 4, 6, and 8 cm, respectively, measured from the cathode surface. The Rogowski coil was set to monitor the time derivative of the discharge current. Signals were recorded using a TDS 540A Textronix digital oscilloscope which has a sampling rate of 1 GS/s and an analog bandwidth of 500 MHz.

Measurements were performed in nitrogen at filling pressures of 0.5 and 1 mbar, respectively. Typical measured signals are illustrated in Fig. 3 for 0.5 (left) and 1 mbar (right).

The corresponding speeds were calculated through linear fits of the measured arrival times (i.e., the time of maximum magnetic probe signal). The mean axial speed of the current sheath u was determined for each filling pressure by measuring the arrival time of the sheath to different axial positions of the magnetic probe. The typical velocities were about 6.2 ± 0.1 and 5.7 ± 0.1 cm/μs for 0.5 and 1 mbar, respectively.

IV. INFERRED CURRENT DENSITY PROFILES

Figure 4 shows, with full lines, typical current density profiles obtained from magnetic probe signals recorded for 0.5 (left) and 1 mbar (right), respectively. The four vertical subplots in each column correspond to the tested vertical positions of the sensing coil (2, 4, 6, and 8 cm, from top to bottom, respectively). In each case, the probe signal is shown in dashed lines. All the signals were normalized to their corresponding maximum for ease of comparison. The results show how the current density structure change as the sheath moves toward the anode tip.

A remarkable feature is that, for both pressures, the current distribution presents two distinct peaks that change their relative amplitude during the evolution of the discharge.

Figure 5 shows the uncertainty in the inferred current density due to geometrical uncertainties in the probe's radius (estimated as 10% of its nominal value), the coil position with respect to the probe tip z_o (7%), and the plasma sheath velocity u (2%), for the second subplot of the second column of Fig. 4 (filling pressure $p=1$ mbar and probe position $h=4$ cm). The error bands were determined by means of the Monte Carlo method,[22] which comprises the following steps. Once all the mentioned geometrical quantities are randomly perturbed within their corresponding uncertainties, a new current density is calculated and stored. This process is repeated 1000 times and then the resulting current densities are plotted together. The error bands reported in Fig. 5 are the borders of such plot.

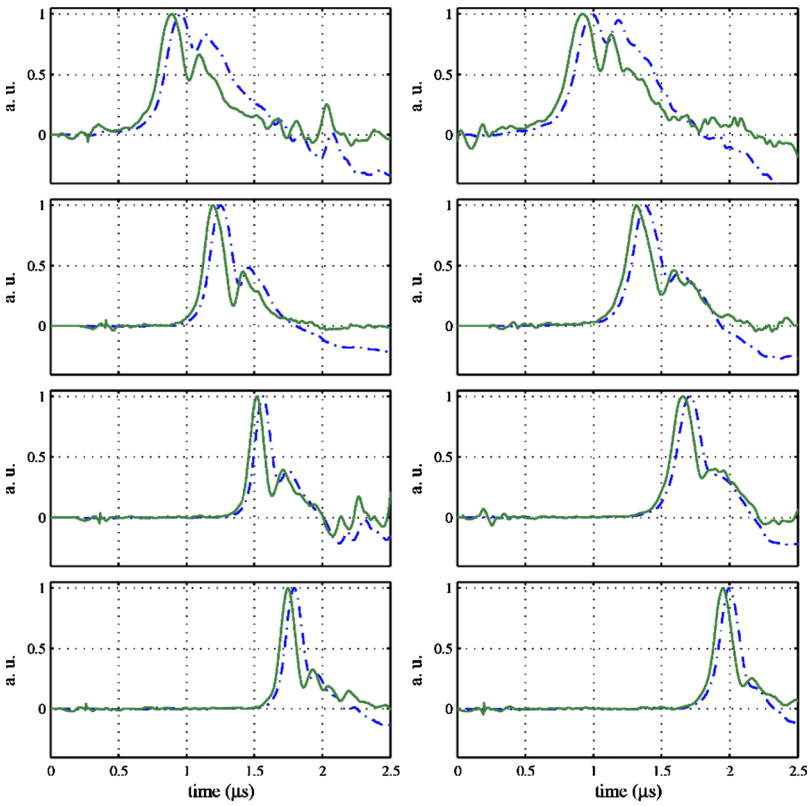

FIG. 4. (Color online) Measured magnetic probe signal (dashed lines) and their corresponding current densities (full lines) for N_2 at 0.5 (left) and 1 mbar (right).

Figure 6 shows the uncertainty in the same case of Fig. 5 due to uncertainties of 5% in the recorded probe signal. The corresponding error bands were determined following the already mentioned Monte Carlo method. Finally, Fig. 7 shows the errors bands due to all the considered uncertainties, which are within 15% of the calculated current density, being the error in the recorded probe signal the dominant contribution.

V. FINAL REMARKS

The current density structure of the running sheath in plasma focus discharges was studied by means of the voltage signal of an inductive probe, while the circuit current derivative was recorded by a Rogowski coil. The signals were analyzed using a theoretical model accounting for the temporal variation of the discharge current and the perturbations introduced by the probe's encasing body. Since the model includes both effects simultaneously, it can be used in a wide variety of experimental situations avoiding the necessity of making specific approximations to ignore such effects.

Although the probe signal gives a qualitative estimation of the general current density structure and width, the calculated profile resolves more adequately the diverse features of the current density structure.

The results show that the width of the current density distribution decreases as the sheath evolves toward the open end of the electrodes. Furthermore, a complex structure was found in the current density distribution profile, presenting at least two spatial maxima.

ACKNOWLEDGMENTS

This research was supported by PLADEMA–CNEA, Universidad de Buenos Aires, and CONICET. P.K. is a doctoral fellow of CONICET. C.M. and A.C. are members of CONICET.

APPENDIX: NUMERICAL SCHEMES

The current density j_x can be numerically inferred from expression (6), discretizing the integral on the right member of the equality. The implemented methodology on this paper, as well as an alternative procedure, are briefly discussed on this section.

1. Numerical method

Redefining the variable z as $z=z_f-\zeta$, the expression (6) can be conveniently rewritten as

$$\frac{\tilde{\nu}(t)}{a(t)} - \frac{\dot{a}(t)}{a^2(t)}\int_0^t \tilde{\nu}(\tau)d\tau = \int_0^{z_f} j_x(-\zeta)\tilde{M}(z_f-\zeta,z_o)d\zeta, \quad \text{(A1)}$$

where the variable ζ is positive defined on the $\hat{z}$ direction, and the function $j_x(-\zeta)$ represents the undisturbed current density. For the sake of notation simplicity, the left member of Eq. (A1) will be referred hereafter as $\nu^*(t)$

$$\nu^*(t) = \int_0^{z_f} j_x(-\zeta)\tilde{M}(z_f-\zeta,z_o)d\zeta. \quad \text{(A2)}$$

2. The matrix approach

To solve Eq. (A2), the integration interval $(0,z_f)$ was divided into N equal subintervals $\delta z=(z_{k-1},z_k)$; being

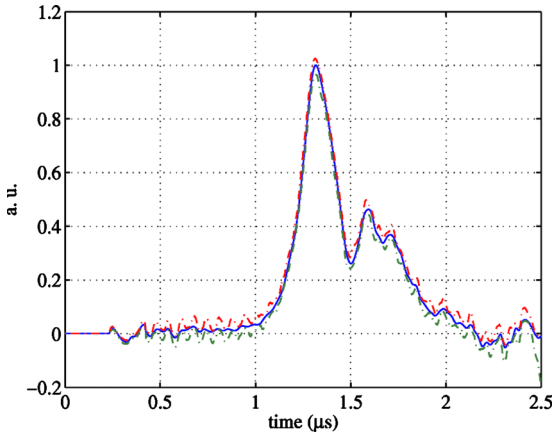

FIG. 5. (Color online) Errors due to the following uncertainties: 10% in the probe's radius, 7% in z_o, and 2% in the plasma sheath velocity u. The discharge was performed in N_2 at 1 mbar and the probe's coil was located at $Z=4$ cm.

$k=1,\cdots,N$. Assuming the unknown current density to be constant on the kth element, the expression (A2) becomes

$$\nu_i^* = \sum_{k=1}^{i} j_k \int_{z_{k-1}}^{z_k} \tilde{M}(z_i - \zeta)d\zeta, \tag{A3}$$

where $1 \le i \le N$, since $\nu(0) = 0$ and j_k represents the current density of the kth considered element. Equation (A3) establishes $k \le i \,\forall\, 1 \le i \le N$, therefore the coefficients M_{ik} of a $N \times N$ lower triangular matrix can be defined as follows

$$M_{ik} \equiv \int_{z_{k-1}}^{z_k} \tilde{M}(z_i - \zeta)d\zeta. \tag{A4}$$

Considering the variable $\varsigma = \zeta - z_{k-1}$ in Eq. (A4), it is possible to verify that the unknown matrix elements are N and that they are related by

$$M_{ik} = M_{i+1-k1} \,\forall\, k \le i, \quad 1 \le i \le N. \tag{A5}$$

Finally, Eqs. (A3)–(A5) set leads to the following linear system:

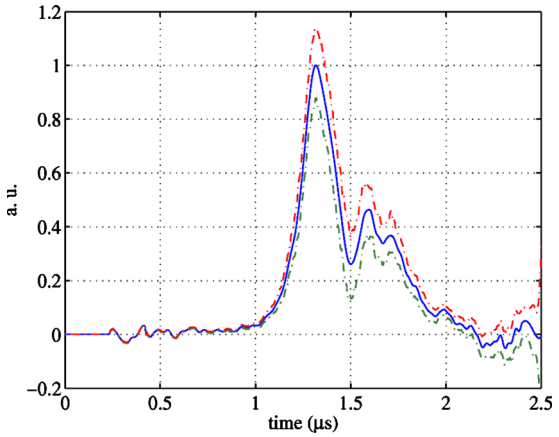

FIG. 6. (Color online) Errors due to uncertainties of 5% in the recorded signal. Same conditions as in Fig. 5.

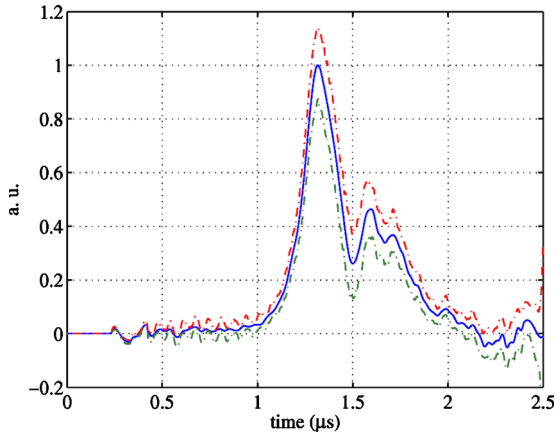

FIG. 7. (Color online) Total error. Same conditions as in Fig. 5.

$$\nu_i^* = \sum_{k=1}^{i} j_k M_{i+1-k1} \tag{A6}$$

which can be equivalently solved either by an iterative method or by inverting matrix M.[23]

From Eq. (A6), and under the assumption that $M_{11} \neq 0$, the current density results to

$$j_i = \frac{\nu_i^* - \Sigma_{k=1}^{i-1} \nu_k^* M_{i+1-k1}}{M_{11}}. \tag{A7}$$

3. The least-squares approach

A least-squares method is also suitable to invert the first kind Volterra equation presented in Eq. (A2). The function to be minimized, χ^2, is

$$\chi^2 = \sum_{z_i} \left[\nu_i^* - \int_0^{z_i} j_x(-\zeta)\tilde{M}(z_i - \zeta, z_0)d\zeta \right]^2, \tag{A8}$$

where the first term inside the parenthesis corresponds to experimental data and the second one represents the theoretical description of them.

Again, the current density is assumed to be constant on each element $\delta z = (z_{k-1}, z_k)$. Since $z_i = i\delta z$ for $1 \le i \le N$, Eq. (A8) can be written as follows

$$\chi^2 = \sum_{i=1}^{N} \left[\nu_i^* - \int_0^{z_i} j_x(-\zeta)\tilde{M}(z_i - \zeta, z_0)d\zeta \right]^2. \tag{A9}$$

From the discretization of the integral on Eq. (A9), the expression (A10) is obtained.

$$\chi^2 = \sum_{i=1}^{N} \left(\nu_i^* - \sum_{k=1}^{i} j_k M_{i+1-k1} \right)^2. \tag{A10}$$

Considering the j_r derivative of the above equation, a set of N homogeneous linear equations can be constructed. The system of linear algebraic equations to be solved to infer the current density is

$$\sum_{i=r}^{N} \left(\nu_i^* M_{i+1-r1} - \sum_{k=1}^{i} j_k M_{i+1-k1} M_{i+1-r1} \right) = 0. \tag{A11}$$

Since, under the assumption that $M_{11} \neq 0$, M has a non-

zero determinant, it verifies that $(M^TM)^{-1}=M^{-1}(M^T)^{-1}$. Considering this property in Eq. (A11), the obtained expression for j_k is in agreement with expression (A7). Therefore, the least-squares formulation is an alternative to the above discussed matrix approach.

[1] P. Lee, X. Feng, G. X. Zhang, M. H. Liu, and S. Lee, Plasma Sources Sci. Technol. **6**, 343 (1997).
[2] S. Lee, P. Lee, G. Zhang, X. Feng, V. A. Gribkov, M. Liu, A. Serban, and T. K. S. Wong, IEEE Trans. Plasma Sci. **26**, 1119 (1998).
[3] V. A. Gribkov, A. Srivastava, P. L. C. Keat, V. Kudryashov, and S. Lee, IEEE Trans. Plasma Sci. **30**, 1331 (2002).
[4] D. Wong, T. L. Tan, A. Patran, S. S. M. Hassan, T. Zhang, S. V. Springham, S. Lee, R. S. Rawat, and P. Lee, in *Proceedings of the Sixth International Conference on Dense Z-Pinches* (AIP, New York, 2006), Vol. 808, pp. 227–230.
[5] H. Kelly, A. Lepone, A. Márquez, D. Lamas, and C. Oviedo, Plasma Sources Sci. Technol. **5**, 704 (1996).
[6] S. Zeb, M. Sadiq, A. Qayyum, G. Murtaza, and M. Zakaullah, Mater. Chem. Phys. **103**, 235 (2007).
[7] S. Zeb, A. Qayyum, M. Shafiq, and M. Zakaullah, Eur. Phys. J.: Appl. Phys. **42**, 145 (2008).
[8] I. A. Khan, M. Hassan, T. Hussain, R. Ahmad, M. Zakaullah, and R. S. Rawat, Appl. Surf. Sci. **255**, 6132 (2009).
[9] M. Zakaullah, K. Alamgir, M. Shafiq, M. Sharif, A. Waheed, and G. Murtaza, J. Fusion Energy **19**, 143 (2000).
[10] F. Castillo-Mejia, M. M. Milanese, R. L. Moroso, J. O. Pouzo, and M. A. Santiago, IEEE Trans. Plasma Sci. **29**, 921 (2001).
[11] C. Moreno, M. Vénere, R. Barbuzza, M. del Fresno, R. Ramos, H. Bruzzone, P. Florido, J. González, and A. Clausse, Braz. J. Phys. **32**, 20 (2002).
[12] S. Hussain, M. Shafiq, R. Ahmad, A. Waheed, and M. Zakaullah, Plasma Sources Sci. Technol. **14**, 61 (2005).
[13] C. Moreno, V. Raspa, L. Sigaut, R. Vieytes, and A. Clausse, Appl. Phys. Lett. **89**, 091502 (2006).
[14] F. Castillo, I. Gamboa-Debuen, J. J. E. Herrera, J. Rangel, and S. Villalobos, Appl. Phys. Lett. **92**, 051502 (2008).
[15] Ye. P. Bogolubov, M. V. Koltunov, B. D. Lemeshko, V. I. Mikerov, V. N. Samosyuk, P. P. Sidorov, and D. I. Yurkov, Nucl. Instrum. Methods Phys. Res. A **605**, 62 (2009).
[16] V. A. Gribkov, in *Proceedings of the Plasma and Fusion Science 17th IAEA Technical Meeting on Research Using Small Fusion Devices* (AIP, New York, 2008), Vol. 996, p. 51.
[17] H. Bruzzone, C. Moreno, and H. Kelly, Meas. Sci. Technol. **2**, 1195 (1991).
[18] L. Bilbao and D. Grondona, Meas. Sci. Technol. **5**, 288 (1994).
[19] H. Bruzzone and D. Grondona, Plasma Phys. Controlled Fusion **39**, 1315 (1997).
[20] J. H. Malmberg, Rev. Sci. Instrum. **35**, 1622 (1964).
[21] P. Linz, *Analytical and Numerical Methods for Volterra Equations* (SIAM, Philadelphia, 1985).
[22] W. H. Press, S. A. Teukolsky, W. T. Vetterling, and B. P. Flannery, *Numerical Recipes in Fortran. The Art of Scientific Computing* (Cambridge University Press, New York, 1992).
[23] See supplementary material at http://dx.doi.org/10.1063/1.3480556 for a MATLAB script that evaluates the current density from measured magnetic probe and Rogowski signals and for an example that uses experimental signals.